Emergent singular solutions of nonlocal density-magnetization equations in one dimension

Darryl D. Holm,[1,2] Lennon Ó Náraigh,[1,*] and Cesare Tronci[1,3]
[1]*Department of Mathematics, Imperial College London, London, SW7 2AZ, United Kingdom*
[2]*Computer and Computational Science Division, Los Alamos National Laboratory, Los Alamos, New Mexico, 87545, USA*
[3]*TERA Foundation for Oncological Hadrontherapy, 11 V. Puccini, Novara 28100, Italy*
(Received 13 November 2007; revised manuscript received 5 February 2008; published 18 March 2008)

We investigate the emergence of singular solutions in a nonlocal model for a magnetic system. We study a modified Gilbert-type equation for the magnetization vector and find that the evolution depends strongly on the length scales of the nonlocal effects. We pass to a coupled density-magnetization model and perform a linear stability analysis, noting the effect of the length scales of nonlocality on the system's stability properties. We carry out numerical simulations of the coupled system and find that singular solutions emerge from smooth initial data. The singular solutions represent a collection of interacting particles (clumpons). By restricting ourselves to the two-clumpon case, we are reduced to a two-dimensional dynamical system that is readily analyzed, and thus we classify the different clumpon interactions possible.

DOI: 10.1103/PhysRevE.77.036211 PACS number(s): 89.75.Kd, 68.55.A−

I. INTRODUCTION

In recent years, the modeling of nanoscale physics has become important, both because of industrial applications [1–4], and because of the development of experiments that probe these small scales [5]. One particular problem is the modeling of aggregation, in which microscopic particles collapse under the potential they exert on each other, and form mesoscopic structures that in turn behave like particles.

In a series of papers, Holm, Putkaradze, and Tronci [6–11] have focused on the derivation of aggregation equations that possess emergent singular solutions. Continuum aggregation equations have been used to model gravitational collapse and the subsequent emergence of stars [12], the localization of biological populations [13–15], and the self-assembly of *nanoparticles* [16]. These are complexes of atoms or molecules forming mesoscale structures with particlelike behavior. In particular, Holm and Putkaradze have shown [10,11] how several aggregation and self-assembly phenomena can be modeled by a continuity equation for the particle density $\rho(\boldsymbol{x},t)$ of the form

$$\frac{\partial\rho}{\partial t}=\mathrm{div}(\rho\mu[\rho]\nabla\Phi[\rho]+D\nabla\rho),$$

where Φ is the collective potential (e.g., $\Delta\Phi=\rho$, for gravitational interactions), while the mobility μ is related to the typical dimension of the particles. The role of friction is fundamental to this model, which is proposed for applications in highly dissipative systems. When the diffusion coefficient D is set equal to zero, this equation becomes a characteristic equation of the form

$$\frac{d}{dt}\rho_t=0 \quad \text{along } \dot{\boldsymbol{x}}_t=-\mu\nabla\Phi.$$

This states that for friction-dominated systems the velocity can be assumed as proportional to the collective force ($V\propto -\nabla\Phi$). This model is often referred to as Darcy's law, and it appears as a unifying principle for a wide range of aggregation phenomena at different scales. The utility of the Holm-Putkaradze model lies in its emphasis on nonlocal physics, and the emergence of singular solutions from smooth initial data. Because of the singular (delta function) behavior of the model, it is an appropriate way to describe the universal phenomena of aggregation and the subsequent formation of particlelike structures. Indeed in this framework, it is possible to prescribe the dynamics of the particlelike structures after collapse. Thus, the model provides a description of directed self-assembly in nanophysics [16,17], in which the detailed physics is less important than the effective medium properties of the dynamics. In this work we focus on equations introduced by Holm, Putkaradze, and Tronci for the aggregation of oriented (or polarized) particles [6,9].

Anisotropic interactions often appear in several contexts, especially in nanotechnology, where the dynamics of magnetic particles is also considered. The model proposed in [6,9] extends Darcy's law to recover the dissipative Gilbert dynamics for the evolution of the magnetization vector in a ferromagnetic medium. This model describes physical systems exhibiting not only aggregation (as in ordinary Darcy's law), but also alignment phenomena. Possible applications can be considered in nanosciences and protein folding, when the relative orientation of molecules plays a crucial role in the dynamics leading to the final configuration. In formulas, one has the following equations for the density ρ and the polarization $\boldsymbol{m}$:

$$\frac{\partial\rho}{\partial t}=\mathrm{div}\left[\rho\left(\mu_\rho\nabla\frac{\delta E}{\delta\rho}+\boldsymbol{\mu}_m\cdot\nabla\frac{\delta E}{\delta\boldsymbol{m}}\right)\right] \tag{1a}$$

and

$$\frac{\partial\boldsymbol{m}}{\partial t}=\mathrm{div}\left[\boldsymbol{m}\otimes\left(\mu_\rho\nabla\frac{\delta E}{\delta\rho}+\boldsymbol{\mu}_m\cdot\nabla\frac{\delta E}{\delta\boldsymbol{m}}\right)\right]+\boldsymbol{m}\times\left(\boldsymbol{\mu}_m\times\frac{\delta E}{\delta\boldsymbol{m}}\right), \tag{1b}$$

where $E(\rho,\boldsymbol{m})$ is the energy functional of the system and

*Corresponding author. lennon.o-naraigh@imperial.ac.uk

$\delta E/\delta\rho$, $\delta E/\delta \boldsymbol{m}$ are its functional derivatives (e.g. in Darcy's law, one has $\Phi = \delta E/\delta\rho$). This paper focuses on the analogy with magnetization dynamics and compares the model with the Gilbert equation. We present some features of this system, which is known [18] to possess singular solutions of the form

$$\rho(\boldsymbol{x},t) = \int a(s,t)\delta(\boldsymbol{x}-\boldsymbol{Q}(s,t))ds,$$

$$\boldsymbol{m}(\boldsymbol{x},t) = \int \boldsymbol{b}(s,t)\delta(\boldsymbol{x}-\boldsymbol{Q}(s,t))ds,$$

where the variable s is a curvilinear coordinate on a moving curve, so that the quantities ρ and $\boldsymbol{m}$ are supported on a filament (as it happens in the case of fluids with vortex lines). By analogy, the coordinate s can also be a coordinate on a moving surface, so that the dynamical variables are supported on a "polarized" sheet. Instead of analyzing the behavior of these three-dimensional structures, this paper presents the dynamics of singular solutions in only one dimension so to present the interactions of single oriented particles. Additionally, we treat the initial state of the system as a continuum, a good approximation in nanophysics applications [19].

Because of the analogy with the dissipative Gilbert equation, we refer to the orientation vector in our continuum picture as the *magnetization*. We investigate Eqs. (1) in one dimension numerically, and study their evolution and aggregation properties. One aspect of nonlocal problems, already mentioned in [11], is the effect of competition between the length scales of nonlocality on the system evolution. We shall highlight this effect with a linear stability analysis of the full density-magnetization equations.

This paper is organized as follows. In Sec. II we introduce a nonlocal Gilbert (NG) equation to describe nonlocal interactions in a magnetic system. We investigate the competition between the system's two length scales of nonlocality. In Sec. III we introduce a coupled density-magnetization system that generates singular solutions. We examine the competition of length scales through a linear stability analysis and through the study of the dynamical equations for a simple singular solution that describes the interaction of two particlelike objects (clumpons). We perform numerical simulations that highlight the emergence of singular solutions from smooth initial data. We draw our conclusions in Sec. IV.

II. THE NONLOCAL GILBERT EQUATION

In this section we study a magnetization equation that in form is similar to the Gilbert equation, that is, the Landau-Lifshitz-Gilbert equation in the overdamped limit [20,21]. The equation we focus on incorporates nonlocal effects, and was introduced in [6]. We study the evolution and energetics of this equation, and examine the importance of the problem length scales in determining the evolution.

We study the following nonlocal Gilbert (NG) equation:

$$\frac{\partial \boldsymbol{m}}{\partial t} = \boldsymbol{m} \times \left(\boldsymbol{\mu}_m \times \frac{\delta E}{\delta \boldsymbol{m}}\right), \tag{2}$$

where $\boldsymbol{m}$ is the magnetization density, $\boldsymbol{\mu}_m$ is the mobility, defined as

$$\boldsymbol{\mu}_m = (1-\beta^2\partial_x^2)^{-1}\boldsymbol{m},$$

and $\delta E/\delta \boldsymbol{m}$ is the variational derivative of the energy,

$$\frac{\delta E}{\delta \boldsymbol{m}} = (1-\alpha^2\partial_x^2)^{-1}\boldsymbol{m}.$$

The meaning of the length scales α and β is related to the physical nature of the quantities E and $\boldsymbol{\mu}_m$. Indeed, the expression given for $\delta E/\delta \boldsymbol{m}$ represents a potential energy $\boldsymbol{\Omega}[\boldsymbol{m}]$ obeying the Helmholtz equation $(1-\alpha^2\Delta)\boldsymbol{\Omega} = \boldsymbol{m}$. Thus, the parameter α represents the characteristic interaction length that regulates magnetization dynamics. For the mobility $\boldsymbol{\mu}_m$, a different argument holds. In the ordinary Gilbert equation, this quantity is proportional to the magnetization, $\boldsymbol{\mu}_m \propto \boldsymbol{m}$. However this choice does not give any information about the magnetic-moment dynamics of the single particle, or, in other terms, this choice does not allow for the oriented single-particle solution. On the other hand, it is possible that the magnetization can reach a configuration where aligned jammed structures interact with each other after their formation and such a configuration is analogous to the interaction among single particles in the system. Consequently, the meaning of the mobility $\boldsymbol{\mu}_m$ is an averaging process that accommodates more than one length scale in order to allow the single-particle dynamics as a solution. The length scale β appearing in the smoothing process is therefore related to the size of the aligned jammed states, or simply the typical length of interacting particles. As we shall see, the particle behavior cannot emerge spontaneously in the nonlocal Gilbert equation. Rather, one could start with an initial set of aligned jammed states so to follow their dynamics. The numerical values of the parameters α and β may depend on several physical quantities, according to the system under consideration. These length scales are in general modeling choices that need to accommodate the experimental results. The smoothened magnetization $\boldsymbol{\mu}_m$ and the force $\delta E/\delta \boldsymbol{m}$ can be computed using the theory of Green's functions. In particular,

$$\boldsymbol{\mu}_m(x,t) = \int_\Omega dy H_\beta(x-y)\boldsymbol{m}(y,t) := H_\beta * \boldsymbol{m}(x,t).$$

Here $*$ denotes the convolution of functions, and the kernel $H_\beta(x)$ satisfies the equation

$$\left(1-\beta^2\frac{d^2}{dx^2}\right)H_\beta(x) = \delta(x). \tag{3}$$

The function $\delta(x)$ is the Dirac delta function. Equation (3) is solved subject to conditions imposed on the boundary of the domain Ω. In this paper we shall work with a periodic domain $\Omega = [-L/2, L/2]$ or $\Omega = [0, L]$, although other boundary conditions are possible. Periodic boundary conditions are justified by the purpose of this section, which presents a nonlocal version of the Gilbert equation. The numerical simulations show the comparison with the results of the local case ($\beta \to 0$). This comparison is *not* affected by the conditions at the boundaries and the physical configuration can be easily interpreted in terms of a magnetized ring undergoing Gilbert dynamics. Note that Eq. (2) has a family of nontrivial equilibrium states given by

$$\boldsymbol{m}_{\rm eq}(x) = \boldsymbol{m}_0 \sin(kx + \phi_0),$$

where $\boldsymbol{m}_0$ is a constant vector, k is some wave number, and ϕ_0 is a constant phase. The derivation of this solution is subject to the boundary conditions discussed in Sec. III. However, periodic solutions are generic solutions of simple nonlocal models [22]. By setting $\beta=0$ and replacing $(1-\alpha^2\partial_x^2)^{-1}$ with $-\partial_x^2$, we recover the more familiar Landau-Lifshitz-Gilbert equation, in the overdamped limit [20],

$$\frac{\partial \boldsymbol{m}}{\partial t} = -\boldsymbol{m} \times \left(\boldsymbol{m} \times \frac{\partial^2 \boldsymbol{m}}{\partial x^2}\right). \tag{4}$$

Equation (2) possesses several features that will be useful in understanding the numerical simulations. There is an energy functional

$$E(t) = \frac{1}{2}\int_\Omega dx \boldsymbol{m} \cdot (1-\alpha^2\partial_x^2)^{-1}\boldsymbol{m}, \tag{5}$$

which evolves in time according to the relation

$$\begin{aligned}\frac{dE}{dt} &= \int_\Omega dx[\boldsymbol{\mu}_m \cdot (1-\alpha^2\partial_x^2)^{-1}\boldsymbol{m}][\boldsymbol{m}\cdot(1-\alpha^2\partial_x^2)^{-1}\boldsymbol{m}] \\ &\quad - \int_\Omega dx(\boldsymbol{\mu}_m \cdot \boldsymbol{m})[(1-\alpha^2\partial_x^2)^{-1}\boldsymbol{m}]^2, \\ &= -\int_\Omega dx[\boldsymbol{m}\times(1-\alpha^2\partial_x^2)^{-1}\boldsymbol{m}]\cdot[\boldsymbol{\mu}_m \times (1-\alpha^2\partial_x^2)^{-1}\boldsymbol{m}].\end{aligned} \tag{6}$$

This is not necessarily a nonincreasing function of time, although setting $\beta=0$ gives

$$\begin{aligned}\left(\frac{dE}{dt}\right)_{\beta=0} &= \int_\Omega dx[\boldsymbol{m}\cdot(1-\alpha^2\partial_x^2)^{-1}\boldsymbol{m}]^2 \\ &\quad - \int_\Omega dx \boldsymbol{m}^2[(1-\alpha^2\partial_x^2)^{-1}\boldsymbol{m}]^2, \\ &= \int_\Omega dx \boldsymbol{m}^2[(1-\alpha^2\partial_x^2)^{-1}\boldsymbol{m}]^2(\cos^2\varphi - 1) \le 0,\end{aligned} \tag{7}$$

where φ is the angle between $\boldsymbol{m}$ and $(1-\alpha^2\partial_x^2)^{-1}\boldsymbol{m}$. In the special case when $\beta \to 0$, we therefore expect $E(t)$ to be a nonincreasing function of time. On the other hand, inspection of Eq. (6) shows that as $\alpha \to 0$, the energy tends to a constant. Additionally, the magnitude of the vector $\boldsymbol{m}$ is conserved. This can be shown by multiplying Eq. (2) by $\boldsymbol{m}$, and by exploiting the antisymmetry of the cross product. Thus, we are interested only in the orientation of the vector $\boldsymbol{m}$; this can be parametrized by two angles on the sphere: the azimuthal angle $\theta(\boldsymbol{x},t)$, and the polar angle $\phi(\boldsymbol{x},t)$, where

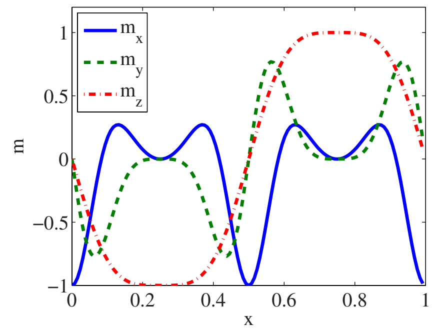

FIG. 1. (Color online) The initial data for the magnetization equation (2). This initialization is obtained by allowing the orientation angles of the magnetization vector to vary sinusoidally in space, as in Eq. (9). Here the wave number of the variation is equal to the fundamental wave number $2\pi/L$.

$$m_x = |\boldsymbol{m}|\cos\phi \sin\theta, \quad m_y = |\boldsymbol{m}|\sin\phi\sin\theta, \quad m_z = |\boldsymbol{m}|\cos\theta, \tag{8}$$

and where $\phi \in [0, 2\pi)$, and $\theta \in [0,\pi]$.

We carry out numerical simulations of Eqs. (2) and (4) on a periodic domain $[0,L]$, and outline the findings in what follows. Motivated by the change of coordinates (8), we choose the initial data

$$\phi_0(x) = \pi(1+\sin(2r\pi x/L)), \quad \theta_0(x) = \frac{1}{2}\pi(1+\sin(2\pi s x/L)), \tag{9}$$

where r and s are integers. These data are shown in Fig. 1.

Case 1: Numerical simulations of Eq.(4). Equation (4) is usually solved by explicit or implicit finite differences [21]. We solve the equation by these methods, and by the explicit spectral method [23]. The accuracy and computational cost is roughly the same in each case, and for simplicity, we therefore employ explicit finite differences; it is this method we use throughout the paper. Given the initial conditions (9), each component of the magnetization $\boldsymbol{m}=(m_x,m_y,m_z)$ tends to a constant, the energy

$$E = \frac{1}{2}\int_\Omega dx \left|\frac{\partial \boldsymbol{m}}{\partial x}\right|^2$$

decays with time, and $|\boldsymbol{m}|^2$ retains its initial value $|\boldsymbol{m}|^2=1$. After some transience, the decay of the energy functional becomes exponential in time. These results are shown in Fig. 2

Case 2: Numerical simulations of Eq.(2) with $\alpha<\beta$. Given the smooth initial data (9), in time each component of the magnetization $\boldsymbol{m}=(m_x,m_y,m_z)$ decays to zero, while the energy

$$E = \frac{1}{2}\int_\Omega dx \boldsymbol{m}\cdot(1-\alpha^2\partial_x^2)^{-1}\boldsymbol{m}$$

tends to a constant value. Given our choice of initial condi-

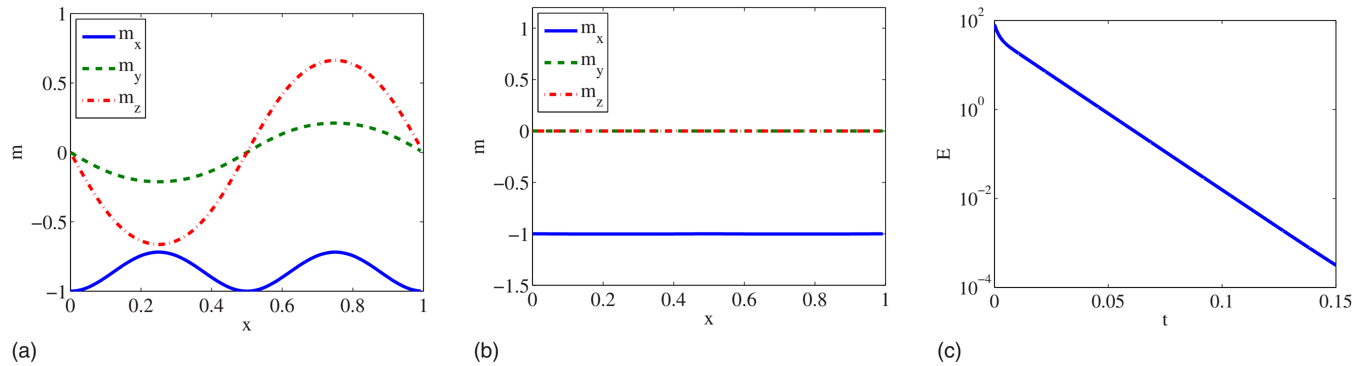

FIG. 2. (Color online) Numerical simulations of Case 1, the Landau-Lifshitz-Gilbert equation in the overdamped limit. In this case, the magnetization decays to a constant state. (a) and (b) show the magnetization at times $t=0.03$ and $t=0.15$, respectively; (c) is the energy functional, which exhibits exponential decay after some transience. The final orientation is $(\phi,\theta)=(\pi,\pi/2)$.

tions, the energy in fact *increases* to attain this constant value. Again the quantity $|\boldsymbol{m}|^2$ stays constant. These results are shown in Fig. 3. We find similar results when we set $\alpha=0$.

Case 3: Numerical simulations of Eq. (2) *with* $\alpha>\beta$. Given the smooth initial data (9), in time each component of the magnetization $\boldsymbol{m}=(m_x,m_y,m_z)$ develops finer and finer scales. The development of small scales is driven by the decreasing nature of the energy functional, which decreases as a power law at late times, and is reflected in snapshots of the power spectrum of the magnetization vector, shown in Fig. 4. As the system evolves, there is a transfer of large amplitudes to higher wave numbers. This transfer slows down at late times, suggesting that the rate at which the solution roughens tends to zero, as $t\to\infty$. The evolution preserves the symmetry of the magnetization vector $\boldsymbol{m}(x,t)$ under parity transformations. This is seen by comparing Figs. 1 and 4. The energy is a decaying function of time, while the quantity $|\boldsymbol{m}|^2$ stays constant. We find similar results for the case when $\beta=0$.

These results can be explained qualitatively as follows. In Case (1), the energy functional exacts a penalty for the formation of gradients. The energy decreases with time and the the system evolves into a state in which no magnetization gradients are present, that is, a constant state. On the other hand, we have demonstrated that in Case (2), when $\alpha<\beta$, the energy increases to a constant value. Since in the nonlocal model, the energy functional represents the cost of forming smooth spatial structures, an increase in energy produces a smoother magnetization field, a process that continues until the magnetization reaches a constant value. Finally, in Case (3), when $\alpha>\beta$, the energy functional decreases, and this decrease corresponds to a roughening of the magnetization field, as seen in Fig. 4. In Sec. III we shall show that Case (2) is stable to small perturbations around a constant state, while Case (3) is unstable. Furthermore, we note that Case (2) and Case (3) differ only by a minus sign in Eq. (2), and are therefore related by time reversal. These results are summarized in Table I.

The solutions of Eqs. (2) and (4) do not become singular. This is not surprising: the manifest conservation of $|\boldsymbol{m}|^2$ in Eqs. (2) and (4) provides a pointwise bound on the magnitude of the solution, preventing blowup. Any addition to Eq. (2) that breaks this conservation law gives rise to the possibility of singular solutions, and it is to this possibility that we now turn.

III. COUPLED DENSITY-MAGNETIZATION EQUATIONS

In this section we study a coupled density-magnetization equation pair that admit singular solutions. We investigate the linear stability of the equations and examine the condi-

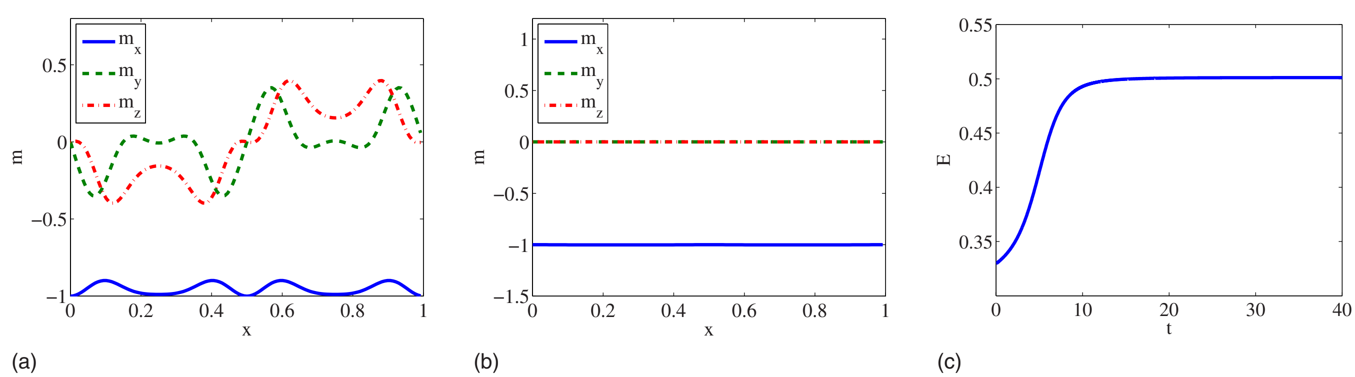

FIG. 3. (Color online) Numerical simulations of Case (2), the nonlocal Gilbert equation with $\alpha<\beta$. In this case, the energy increases to a constant value, and the magnetization becomes constant. (a) and (b) show the magnetization at times $t=8$ and $t=40$; (c) is the energy functional. The final orientation is $(\phi,\theta)=(\pi,\pi/2)$.

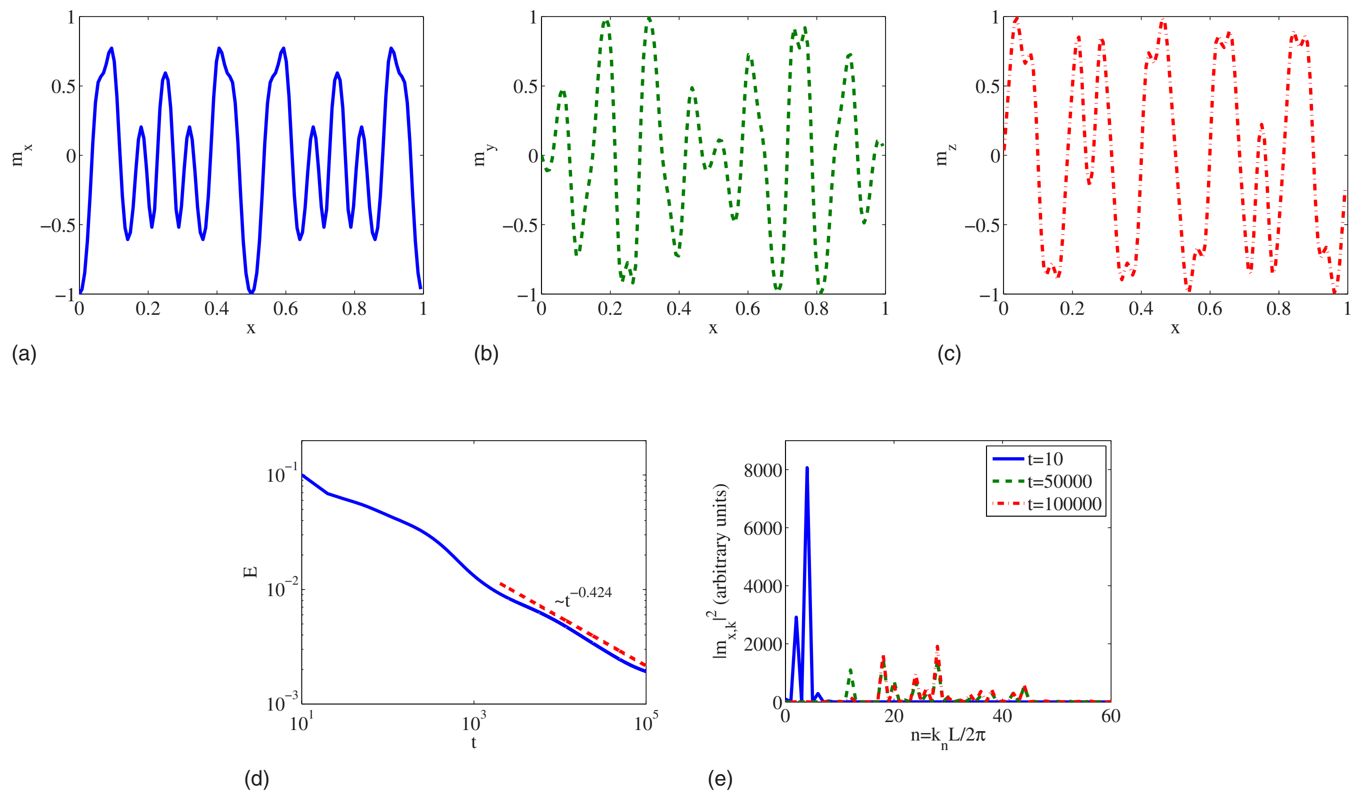

FIG. 4. (Color online) Numerical simulations of Case 3, the nonlocal Gilbert equation with $\alpha > \beta$. In this case, the energy decreases indefinitely, and the magnetization vector develops finer and finer scales. (a), (b), and (c) show the magnetization at time $t = 10000$; (d) is the energy functional, which decreases in time as a power law at late times. (e) shows the power spectrum of m_x; the integer index n labels the spatial scales: if k_n is a wave number, then the corresponding integer label is $n = k_n L/2\pi$.

tions for instability. We find that the stability or otherwise of a constant state is controlled by the magnetization and density values of that state, and by the relative magnitude of the problem length scales. Using numerical and analytical techniques, we investigate the emergence and self-interaction of singular solutions.

The equations we study are as follows:

$$\frac{\partial \rho}{\partial t} = \frac{\partial}{\partial x}\left[\rho\left(\mu_\rho \frac{\partial}{\partial x}\frac{\delta E}{\delta \rho} + \boldsymbol{\mu}_m \cdot \frac{\partial}{\partial x}\frac{\delta E}{\delta \boldsymbol{m}}\right)\right], \tag{10a}$$

$$\frac{\partial \boldsymbol{m}}{\partial t} = \frac{\partial}{\partial x}\left[\boldsymbol{m}\left(\mu_\rho \frac{\partial}{\partial x}\frac{\delta E}{\delta \rho} + \boldsymbol{\mu}_m \cdot \frac{\partial}{\partial x}\frac{\delta E}{\delta \boldsymbol{m}}\right)\right] + \boldsymbol{m} \times \left(\boldsymbol{\mu}_m \times \frac{\delta E}{\delta \boldsymbol{m}}\right), \tag{10b}$$

where we set

$$\mu_\rho = 1, \quad \frac{\delta E}{\delta \rho} = -(1 - \alpha_\rho^2 \partial_x^2)^{-1}\rho, \tag{11a}$$

and, as before,

$$\boldsymbol{\mu}_m = (1 - \beta_m^2 \partial_x^2)^{-1}\boldsymbol{m}, \quad \frac{\delta E}{\delta \boldsymbol{m}} = (1 - \alpha_m^2 \partial_x^2)^{-1}\boldsymbol{m}. \tag{11b}$$

These equations have been introduced by Holm, Putkaradze, and Tronci in [6], using a kinetic-theory description. The density and the magnetization vector are driven by the velocity

$$V = \mu_\rho \frac{\partial}{\partial x}\frac{\delta E}{\delta \rho} + \boldsymbol{\mu}_m \cdot \frac{\partial}{\partial x}\frac{\delta E}{\delta \boldsymbol{m}}. \tag{12}$$

The velocity advects the ratio $|\boldsymbol{m}|/\rho$ by

TABLE I. Summary of the forms of Eq. (2) studied.

Case	Length scales	Energy	Outcome as $t \to \infty$	Linear stability
(1)	$\beta = 0,\ \delta E/\delta \boldsymbol{m} = -\partial_x^2 \boldsymbol{m}$	Decreasing	Constant state	Stable
(2)	$\alpha < \beta$	Increasing	Constant state	Stable
(3)	$\alpha > \beta$	Decreasing	Development of finer and finer scales	Unstable

$$\left(\frac{\partial}{\partial t} - V\frac{\partial}{\partial x}\right)\frac{|\boldsymbol{m}|}{\rho} = 0.$$

We have the system energy

$$E = \frac{1}{2}\int_{\Omega} dx\boldsymbol{m}\cdot(1-\alpha_m^2\partial_x^2)^{-1}\boldsymbol{m} - \frac{1}{2}\int_{\Omega} dx\rho(1-\alpha_\rho^2\partial_x^2)^{-1}\rho, \tag{13}$$

and, given a non-negative density, the second term is always nonpositive. This represents an energy of attraction, and we therefore expect singularities in the magnetization vector to arise from a collapse of the particle density due to the ever-decreasing energy of attraction. There are three length scales in the problem that control the time evolution: the ranges α_m and α_ρ of the potentials in Eq. (13), and the smoothening length β_m.

A. Linear stability analysis

We study the linear stability of the constant state $(\boldsymbol{m},\rho) = (\boldsymbol{m}_0,\rho_0)$. We evaluate the smoothened values of this constant solution as follows:

$$(1-\alpha_\rho^2\partial_x^2)^{-1}\rho_0 = f(x),$$

$$\rho_0 = f(x) - \alpha_\rho^2\frac{d^2f}{dx^2},$$

$$f(x) = \rho_0 + A\sinh(x/\alpha_\rho) + B\cosh(x/\alpha_\rho).$$

For periodic or infinite boundary conditions, the constants A and B are in fact zero and thus

$$(1-\alpha_\rho\partial_x^2)^{-1}\rho_0 = \rho_0, \tag{14}$$

and similarly $\boldsymbol{\mu}_0 = (\delta E/\delta \boldsymbol{m})_{\boldsymbol{m}_0} = \boldsymbol{m}_0$. The result (14) guarantees that the constant state $(\boldsymbol{m}_0,\rho_0)$ is indeed a solution of Eq. (10).

We study a solution $(\boldsymbol{m},\rho) = (\boldsymbol{m}_0+\delta\boldsymbol{m},\rho_0+\delta\rho)$, which represents a perturbation away from the constant state. By assuming that $\delta\boldsymbol{m}$ and $\delta\rho$ are initially small in magnitude, we obtain the following linearized equations for the perturbation density and magnetization:

$$\frac{\partial}{\partial t}\delta\rho = -\rho_0\frac{\partial^2}{\partial x^2}(1-\alpha_\rho^2\partial_x^2)^{-1}\delta\rho + \rho_0\frac{\partial^2}{\partial x^2}(1-\alpha_m^2\partial_x^2)^{-1}\boldsymbol{m}_0\cdot\delta\boldsymbol{m},$$

$$\begin{aligned}\frac{\partial}{\partial t}\delta\boldsymbol{m} = \boldsymbol{m}_0\Bigg[&-\frac{\partial^2}{\partial x^2}(1-\alpha_\rho^2\partial_x^2)^{-1}\delta\rho \\ &+\frac{\partial^2}{\partial x^2}(1-\alpha_m^2\partial_x^2)^{-1}\boldsymbol{m}_0\cdot\delta\boldsymbol{m}\Bigg] \\ &+\boldsymbol{m}_0\times\{\boldsymbol{m}_0\times[(1-\alpha_m^2\partial_x^2)^{-1}\delta\boldsymbol{m} - (1-\beta_m^2\partial_x^2)^{-1}\delta\boldsymbol{m}]\}.\end{aligned} \tag{15}$$

For $\boldsymbol{m}_0\neq\boldsymbol{0}$ we may choose two unit vectors $\hat{\boldsymbol{n}}_1$ and $\hat{\boldsymbol{n}}_2$ such that $\boldsymbol{m}_0/|\boldsymbol{m}_0|$, $\hat{\boldsymbol{n}}_1$ and $\hat{\boldsymbol{n}}_2$ form an orthonormal triad (that is, we have effected a change of basis). We then study the quantities $\delta\rho$, $\delta\chi$, $\delta\xi_1$, and $\delta\xi_2$, where

$$\delta\chi = \boldsymbol{m}_0\cdot\delta\boldsymbol{m}, \quad \delta\xi_1 = \hat{\boldsymbol{n}}_1\cdot\delta\boldsymbol{m}, \quad \delta\xi_2 = \hat{\boldsymbol{n}}_2\cdot\delta\boldsymbol{m}.$$

We obtain the linear equations

$$\frac{\partial}{\partial t}\delta\rho = -\rho_0\frac{\partial^2}{\partial x^2}(1-\alpha_\rho^2\partial_x^2)^{-1}\delta\rho + \rho_0\frac{\partial^2}{\partial x^2}(1-\alpha_m^2\partial_x^2)^{-1}\delta\chi,$$

$$\frac{\partial}{\partial t}\delta\chi = -|\boldsymbol{m}_0|^2\frac{\partial^2}{\partial x^2}(1-\alpha_\rho^2\partial_x^2)^{-1}\delta\rho + |\boldsymbol{m}_0|^2\frac{\partial^2}{\partial x^2}(1-\alpha_m^2\partial_x^2)^{-1}\delta\chi,$$

$$\frac{\partial}{\partial t}\delta\xi_i = [(1-\beta_m^2\partial_x^2)^{-1} - (1-\alpha_m^2\partial_x^2)^{-1}]\delta\xi_i, \quad i=1,2.$$

By focusing on a single-mode disturbance with wave number k we obtain the following system of equations:

$$\frac{d}{dt}\begin{pmatrix}\delta\rho\\ \delta\chi\\ \delta\xi_1\\ \delta\xi_2\end{pmatrix} = \begin{pmatrix} \frac{\rho_0k^2}{1+\alpha_\rho^2k^2} & -\frac{\rho_0k^2}{1+\alpha_m^2k^2} & 0 & 0\\ \frac{|\boldsymbol{m}_0|^2k^2}{1+\alpha_\rho^2k^2} & -\frac{|\boldsymbol{m}_0|^2k^2}{1+\alpha_m^2k^2} & 0 & 0\\ 0 & 0 & \frac{1}{1+\beta_m^2k^2}-\frac{1}{1+\alpha_m^2k^2} & 0\\ 0 & 0 & 0 & \frac{1}{1+\beta_m^2k^2}-\frac{1}{1+\alpha_m^2k^2}\end{pmatrix}\begin{pmatrix}\delta\rho\\ \delta\chi\\ \delta\xi_1\\ \delta\xi_2\end{pmatrix},$$

with eigenvalues

$$\sigma_0 = 0, \quad \sigma_1 = \frac{\rho_0 k^2}{1+\alpha_\rho^2 k^2} - \frac{|\boldsymbol{m}_0|^2 k^2}{1+\alpha_m^2 k^2},$$
$$\sigma_2 = \frac{1}{1+\beta_m^2 k^2} - \frac{1}{1+\alpha_m^2 k^2}. \qquad (16)$$

The eigenvalues are the growth rate of the disturbance $(\delta\rho, \delta\chi, \delta\xi_1, \delta\xi_2)$ [24]. There are two routes to instability, when $\sigma_1 > 0$, or when $\sigma_2 > 0$. The first route leads to an instability when

$$\sigma_1 > 0, \quad \frac{\rho_0}{|\boldsymbol{m}_0|^2} > \frac{1+\alpha_\rho^2 k^2}{1+\alpha_m^2 k^2},$$

while the second route leads to instability when

$$\sigma_2 > 0, \quad \alpha_m > \beta_m.$$

Physically, the first route to instability has as its origin the repulsive (negative-definite) contribution to the energy provided by the density ρ, as given by Eq. (11a); on the other hand, the second route to instability derives from the energetically unfavorable nature of a constant magnetization state when $\beta_m < \alpha_m$, as in Sec. II.

We have plotted the growth rates for the case when $\rho_0 = |\boldsymbol{m}_0|^2 = 1$, and compared the theory with numerical simulations. There is excellent agreement at low wave numbers, although the numerical simulations become less accurate at high wave numbers. This can be remedied by increasing the resolution of the simulations. These plots are shown in Figs. 5 and 6. The growth rates $\sigma_{1,2}$ are parabolic in k at small k; σ_1 saturates at large k, while σ_2 attains a maximum and decays at large k. The growth rates can be positive or negative, depending on the initial configuration, and on the relationship between the problem length scales. In contrast to some standard instabilities of pattern formation (e.g., Cahn-Hilliard [25] or Swift-Hohenberg [26]), the σ_1-unstable state becomes more unstable at higher wave numbers (smaller scales), thus preventing the "freezing-out" of the instability by a reduction of the box size [25]. The growth at small scales is limited, however, by the saturation in σ as $k \to \infty$. Heuristically, this can be explained as follows: at higher wave number, the disturbance $(\delta\rho, \delta\chi, \delta\xi_1, \delta\xi_2)$ gives rise to more and more peaks per unit length. This makes merging events increasingly likely, so that peaks combine to form larger peaks, enhancing the growth of the disturbance.

Recall in Sec. II that the different behaviors of the magnetization equation (2) are the result of a competition between the length scales α_m and β_m. For $\alpha_m < \beta_m$ the initial (large-amplitude) disturbance tends to a constant, while for $\alpha_m > \beta_m$ the initial disturbance develops finer and finer scales. In this section, we have shown that the coupled density-magnetization equations are linearly stable when $\alpha_m < \beta_m$, while the reverse case is unstable. In contrast to the first route to instability, the growth rate σ_2, if positive, admits a maximum. This is obtained by setting $\sigma_2'(k) = 0$. Then the maximum growth rate occurs at a scale

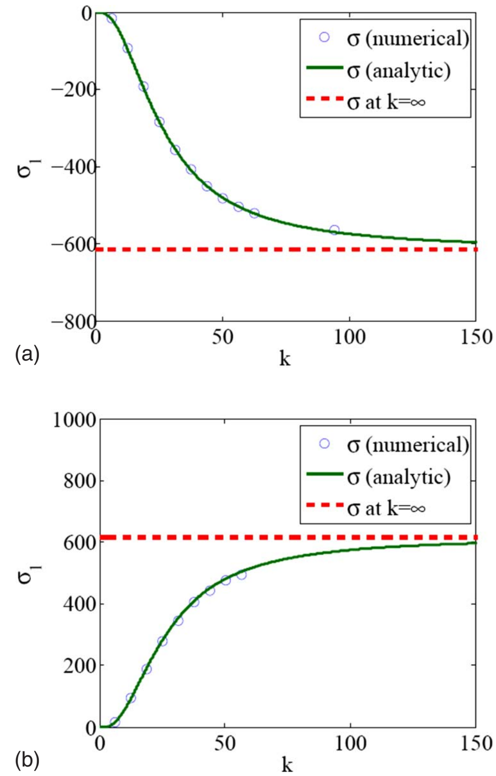

FIG. 5. (Color online) The first route to instability. (a) shows the growth rate σ_1 for $\alpha_m < \beta_m < \alpha_\rho$, with negativity indicating a stable equilibrium; (b) gives the growth rate σ_1 for $\alpha_\rho < \alpha_m < \beta_m$, with positivity indicating an unstable equilibrium. We have set $|\boldsymbol{m}_0| = \rho_0 = 1$.

$$\lambda_{\max} := 2\pi k_{\max}^{-1} = 2\pi\sqrt{\alpha_m \beta_m}.$$

Thus, the scale at which the disturbance is most unstable is determined by the geometric mean of α_m and β_m. Given a disturbance $(\delta\rho, \delta\chi, \delta\xi_1, \delta\xi_2)$ with a range of modes initially present, the instability selects the disturbance on the scale $\lambda_{\max}$. This disturbance develops a large amplitude and a singular solution subsequently emerges. It is to this aspect of the problem that we now turn.

B. Singular solutions

In this section we show that a finite weighted sum of delta functions satisfies the partial differential equations (10). Each delta function has the interpretation of a particle or clumpon, whose weights and positions satisfy a finite set of ordinary differential equations. We investigate the two-clumpon case analytically and show that the clumpons tend to a state in which they merge, diverge, or are separated by a fixed distance. In each case, we determine the final state of the clumpon magnetization.

To verify that singular solutions are possible, let us substitute the ansatz

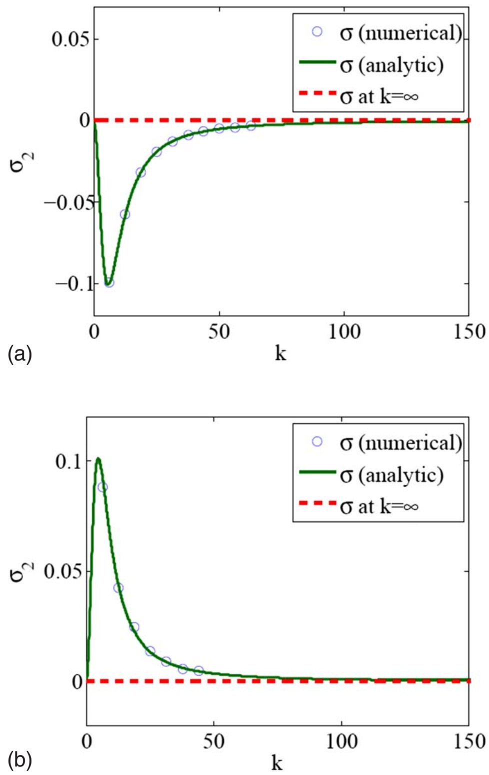

FIG. 6. (Color online) The second route to instability. (a) shows the growth rate σ_2 for $\alpha_m<\beta_m$, with negativity indicating a stable equilibrium; (b) gives the growth rate σ_2 for $\alpha_m>\beta_m$, with positivity indicating an unstable equilibrium. We have set $|\boldsymbol{m}_0|=\rho_0=1$.

$$\rho(x,t)=\sum_{i=1}^{M} a_i(t)\,\delta(x-x_i(t)),\quad \boldsymbol{m}(x,t)=\sum_{i=1}^{M}\boldsymbol{b}_i(t)\,\delta(x-x_i(t)) \tag{17}$$

into the weak form of equations (10). Here we sum over the different components of the singular solution (which we call clumpons). In this section we work on the infinite domain $x\in(-\infty,\infty)$. The weak form of the equations is obtained by testing Eqs. (10) with once-differentiable functions $\phi(x)$ and $\boldsymbol{\psi}(x)$,

$$\frac{d}{dt}\int_{-\infty}^{\infty} dx\rho(x,t)\phi(x)=-\int_{-\infty}^{\infty} dx\phi'(x,t)\times\left(\mu_\rho\frac{\partial}{\partial x}\frac{\delta E}{\delta\rho}+\boldsymbol{\mu_m}\cdot\frac{\partial}{\partial x}\frac{\delta E}{\delta\boldsymbol{m}}\right), \tag{18a}$$

$$\frac{d}{dt}\int_{-\infty}^{\infty} dx\boldsymbol{m}(x,t)\cdot\boldsymbol{\psi}(x)=-\int_{-\infty}^{\infty} dx\boldsymbol{\psi}'(x)\cdot\boldsymbol{m}(x,t)\times\left(\mu_\rho\frac{\partial}{\partial x}\frac{\delta E}{\delta\rho}+\boldsymbol{\mu_m}\cdot\frac{\partial}{\partial x}\frac{\delta E}{\delta\boldsymbol{m}}\right)+\int_{-\infty}^{\infty} dx\boldsymbol{\psi}(x)\cdot\left[\boldsymbol{m}\left(\boldsymbol{\mu_m}\times\frac{\delta E}{\delta\boldsymbol{m}}\right)\right], \tag{18b}$$

Substitution of the ansatz (17) into the weak equations (18) yields the relations

$$\frac{da_i}{dt}=0,\quad \frac{dx_i}{dt}=-V(x_i),\quad \frac{d\boldsymbol{b}_i}{dt}=\boldsymbol{b}_i\times\left(\boldsymbol{\mu}\times\frac{\delta E}{\delta\boldsymbol{m}}\right)(x_i),\quad i\in\{1,\ldots,M\}, \tag{19}$$

where V and $(\boldsymbol{\mu}\times(\delta E/\delta\boldsymbol{m}))$ are obtained from the ansatz (17) and are evaluated at x_i. Note that the density weights a_i and the magnitude of the weights $\boldsymbol{b}_i$ remain constant in time.

We develop further understanding of the clumpon dynamics by studying the two-clumpon version of Eqs. (19). Since the weights a_1, a_2, $|\boldsymbol{b}_1|$, and $|\boldsymbol{b}_2|$ are constant, two variables suffice to describe the interaction: the relative separation $x=x_1-x_2$ of the clumpons, and the cosine of the angle between the clumpon magnetizations, $\cos\varphi=\boldsymbol{b}_1\cdot\boldsymbol{b}_2/|\boldsymbol{b}_1||\boldsymbol{b}_2|$. Using the properties of the kernel $H(0)=1$, $H'(0)=0$, we derive the equations

$$\frac{dx}{dt}=MH'_{\alpha_\rho}(x)-B_1H'_{\alpha_m}(x)H_{\beta_m}(x)-B_2H'_{\alpha_m}(x)y,\quad y=\cos\varphi, \tag{20a}$$

$$\frac{dy}{dt}=B_2(1-y^2)[H_{\beta_m}(x)-H_{\alpha_m}(x)], \tag{20b}$$

where $M=a_1+a_2$, $B_1=|\boldsymbol{b}_1|^2+|\boldsymbol{b}_2|^2$, and $B_2=2|\boldsymbol{b}_1||\boldsymbol{b}_2|$ are constants. Equations (20) form a dynamical system whose properties we now investigate using phase-plane analysis [27]. We note first of all that the $|y|>1$ region of the phase plane is forbidden, since the y component of the vector field $(dx/dt,dy/dt)$ vanishes at $|y|=1$. The vertical lines $x=0$ and $x=\pm\infty$ are equilibria, although their stability will depend on the value of the parameters $(\alpha_m,\alpha_\rho,\beta_m,B_1,B_2,M)$. The curve across which dx/dt changes sign is called the nullcline. This is given by

$$y=\frac{MH'_{\alpha_\rho}(x)-B_1H'_{\alpha_m}(x)H_{\beta_m}(x)}{B_2H'_{\alpha_m}(x)},$$

which on the domain $x\in(-\infty,\infty)$ takes the form

$$y=\frac{\alpha_m}{B_2}\left[\frac{M}{\alpha_\rho}e^{-|x|\left(\frac{1}{\alpha_\rho}-\frac{1}{\alpha_m}\right)}-\frac{B_1}{\alpha_m}e^{-\frac{1}{\beta_m}|x|}\right].$$

Several qualitatively different behaviors are possible, depending on the magnitude of the values taken by the parameters $(\alpha_m,\alpha_\rho,\beta_m,B_1,B_2,M)$. Here we outline four of these behavior types.

(i) *Case 1:* The length scales are in the relation $\alpha_m<\alpha_\rho$, and $\beta_m<\alpha_m$. The vector field $(dx/dt,dy/dt)$ and the nullcline are shown in Fig. 7(a). There is flow into the fixed points $(x,y)=(\pm d,1)$, and into the line $x=0$, while y is a nondecreasing function of time, which follows from Eq. (20b). The ultimate state of the system is thus $x=\pm d$, $\varphi=0$ (alignment), or $x=0$ (merging). In the latter case the final orientation is given by the integral of Eq. (20b):

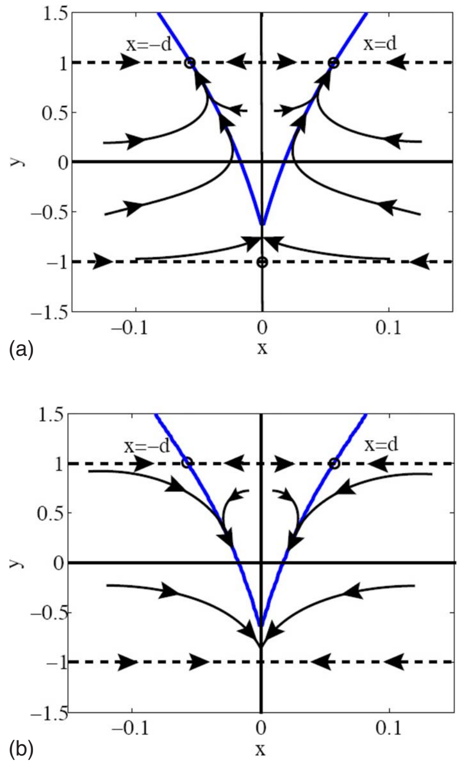

FIG. 7. (Color online) The nullcline $dx/dt=0$ of the two-clumpon dynamical system with $\alpha_m<\alpha_\rho$. The region contained inside the dotted lines $y=\pm 1$ gives the allowed values of the dynamical variables (x,y). (a) shows the case when $\beta_m<\alpha_m$. The stable equilibria of the system are $(x,y)=(\pm d,1)$ and the line $x=0$. All initial conditions flow into one of these equilibrium states; (b) shows the case when $\alpha_m<\beta_m$. Initial conditions confined to the line $y=1$ flow into the fixed point $(\pm d,1)$, while all other initial conditions flow into the line $x=0$.

$$\tan\left(\frac{\varphi}{2}\right)=\tan\left(\frac{\varphi_0}{2}\right)\exp\left[-B_2\int_0^\infty dt\Big[H_{\beta_m}(x(t)) - H_{\alpha_m}(x(t))\Big]\right], \quad \varphi_0=\varphi(t=0). \qquad (21)$$

(ii) *Case 2:* The length scales are in the relation $\alpha_m<\alpha_\rho$, $\alpha_m<\beta_m$. The vector field and the nullcline are shown in Fig. 7(b). All flow not confined to the line $y=1$ is into the line $x=0$, since y is now a nonincreasing function of time. The ultimate state of the system is thus $x=\pm d$, $\varphi=0$ (alignment), or $x=0$ (merging). In the latter case the final orientation is given by the formula (21).

(iii) *Case 3:* The length scales are in the relation $\alpha_\rho<\alpha_m$ and $\beta_m<\alpha_m$. The vector field and the nullcline are shown in Fig. 8(a). Inside the region bounded by the line $y=0$ and the nullcline, the flow is into the line $x=0$ (merging), and the fixed points $(\pm d,1)$ are unstable. The flow below the line $y=0$ is toward the line $x=0$. Outside of these regions, however, the flow is into the lines $x=\pm\infty$, which shows that for a suitable choice of parameters and initial conditions, the clumpons can be made to diverge.

(iv) *Case 4:* The length scales are in the relation $\alpha_\rho<\alpha_m$ and $\alpha_m<\beta_m$. The vector field and the nullcline are shown in Fig. 8(b). The quantity y is a nonincreasing function of time. All flow along the line $y=1$ is directed away from the fixed points $(\pm d,1)$ and is into the fixed points $(0,1)$, or $(\pm\infty,1)$. All other initial conditions flow into $x=0$, although initial conditions that start above the curve formed by the nullcline flow in an arc and eventually reach a fixed point $(x=0,y<0)$.

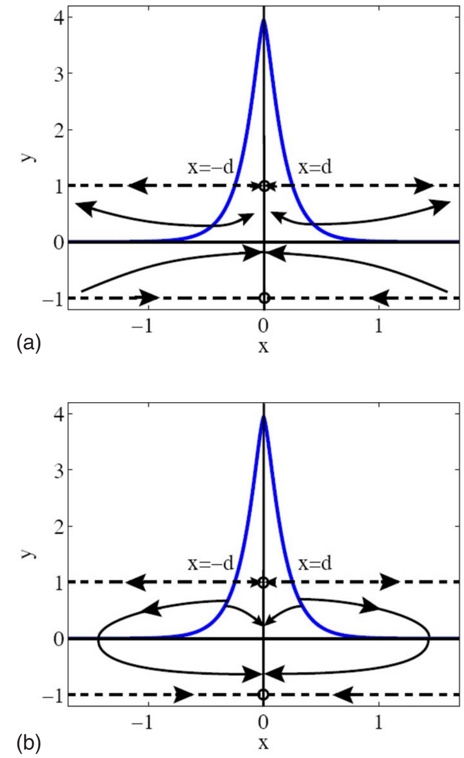

FIG. 8. (Color online) The nullcline $dx/dt=0$ of the two-clumpon dynamical system with $\alpha_\rho<\alpha_m$. The region contained inside the dotted lines $y=\pm 1$ gives the allowed values of the dynamical variables (x,y). (a) shows the case when $\beta_m<\alpha_m$. The lines $x=0$ and $x=\pm\infty$ form the stable equilibria of the system. All initial conditions flow into one of these states; (b) shows the case when $\alpha_m<\beta_m$. Initial conditions confined to the line $y=1$ flow into the fixed points $(0,1)$ and $(\pm\infty,1)$, while all other initial conditions flow into the line $x=0$.

We summarize the cases we have discussed in Table II. Using numerical simulations of Eqs. (20), we have verified that Cases (1)–(4) do indeed occur. The list of cases we have considered is not exhaustive: depending on the parameters B_1, B_2, and M, other phase portraits may arise. Indeed, it is clear from Fig. 7 that through saddle-node bifurcations, the fixed points $(x,y)=(\pm d,1)$ may disappear, or additional fixed points $(x,y)=(\pm d',-1)$ may appear. Our analysis shows, however, that it is possible to choose a set of parameters $(\alpha_\rho,\alpha_m,\beta_m,B_1,B_2,M)$ such that two clumpons either merge, diverge, or are separated by a fixed distance. Although we have studied the relatively simple two-clumpon case, it is an important case to consider, since the clumpon interactions are pairwise; indeed, given the finite range of the interaction, a system with arbitrarily many particles will behave like a collection of isolated particle pairs. We can therefore say that the qualitative late-time behavior of a larger

TABLE II. Summary of the distinct phase portraits of Eq. (20) studied.

Case	α_m vs α_ρ	α_m vs β_m	Equilibria	Flow
(1)	$\alpha_m<\alpha_\rho$	$\beta_m<\alpha_m$	$(x,y)=(\pm d,1)$; $x=0$; $x=\pm\infty$	Flow into $x=0$ and $(x,y)=(\pm d,1)$
(2)	$\alpha_m<\alpha_\rho$	$\alpha_m<\beta_m$	$(x,y)=(\pm d,1)$; $x=0$; $x=\pm\infty$	Flow into $x=0$ and $(x,y)=(\pm d,1)$
(3)	$\alpha_\rho<\alpha_m$	$\beta_m<\alpha_m$	$(x,y)=(\pm d,1)$; $x=0$; $x=\pm\infty$	Flow into $x=0$ and $x=\pm\infty$
(4)	$\alpha_\rho<\alpha_m$	$\alpha_m<\beta_m$	$(x,y)=(\pm d,1)$; $x=0$; $x=\pm\infty$	Flow into $x=0$ and $x=\pm\infty$

system consists of clumpons that execute these three basic behaviors.

C. Numerical simulations

To examine the emergence and subsequent interaction of the clumpons, we carry out numerical simulations of Eq. (10) for a variety of initial conditions. We use an explicit finite-difference algorithm with a small amount of artificial diffusion. We solve the following weak form of Eq. (10), obtained by testing Eq. (18) with H_{β_m}:

$$\frac{\partial\bar{\rho}}{\partial t}=D_{\text{artif}}\frac{\partial^2\bar{\rho}}{\partial x^2}+\int_\Omega dyH'_{\beta_m}(x-y)\rho(y,t)V(y,t),$$

$$\frac{\partial\mu_i}{\partial t}=D_{\text{artif}}\frac{\partial^2\mu_i}{\partial x^2}+\int_\Omega dyH'_{\beta_m}(x-y)\boldsymbol{m}_i(y,t)V(y,t)$$

$$+\int_\Omega dyH_{\beta_m}(x-y)\boldsymbol{e}_i\cdot\left[\boldsymbol{m}\times\left(\boldsymbol{\mu}\times\frac{\delta E}{\delta\boldsymbol{m}}\right)\right],$$

where $\bar{\rho}=H_{\beta_m}*\rho$ and $\boldsymbol{e}_i$ is the unit vector in the i^{th} direction. We work on a periodic domain $\Omega=[-L/2,L/2]$, at a resolution of 250 gridpoints; going to higher resolution does not noticeably increase the accuracy of the results.

The first set of initial conditions we study is the following:

$$\boldsymbol{m}(x,0)=(\sin(4k_0x+\phi_x),\sin(4k_0x+\phi_y),\sin(4k_0x+\phi_z)),$$

$$\rho(x,0)=0.5+0.35\cos(2k_0x), \tag{22}$$

where ϕ_x, ϕ_y, and ϕ_z are random phases in the interval $[0,2\pi]$, and $k_0=2\pi/L$ is the fundamental wave number. The initial conditions for the magnetization vector are chosen to represent the lack of a preferred direction in the problem. The time evolution of equations (10) for this set of initial conditions is shown in Fig. 9. After a short time, the initial data become singular, and subsequently, the solution $(\rho,\boldsymbol{m})$ can be represented as a sum of clumpons,

$$\rho(x,t)=\sum_{i=1}^{M}a_i\delta(x-x_i(t)),$$

$$\boldsymbol{m}(x,t)=\sum_{i=1}^{M}\boldsymbol{b}_i(t)\delta(x-x_i(t)),\quad M=2.$$

Here $M=2$ is the number of clumpons present at the singularity time. This number corresponds to the number of maxima in the initial density profile. The forces exerted by each clumpon on the other balance because of the effect of the periodic boundary conditions. Indeed, any number of equally spaced, identical, interacting particles arranged on a ring are in equilibrium, although this equilibrium is unstable for an attractive force. Thus, at late times, the clumpons are stationary, while the magnetization vector $\boldsymbol{\mu}$ shows alignment of clumpon magnetizations.

We gain further understanding of the formation of singular solutions by studying the system velocity V just before the onset of the singularity. This is done in Fig. 10. Figure 10 (a) shows the development of the two clumpons from the initial data. Across each density maximum, the velocity has the profile $V\approx\lambda(t)x$, where $\lambda(t)>0$ is an increasing function of time. This calls to mind the advection problem for the scalar $\theta(x,t)$, studied by Batchelor in the context of passive-scalar mixing [28]

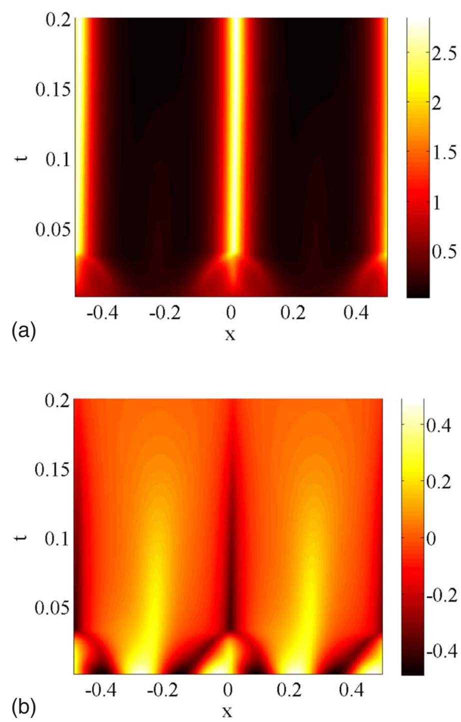

FIG. 9. (Color online) Evolution of sinusoidally varying initial conditions for the density and magnetization, as in Eq. (22). (a) shows the evolution of $H_\rho*\rho$ for $t\in[0,0.15]$, by which time the initial data have formed two clumpons; (b) shows the evolution of μ_x. The profiles of μ_y and μ_z are similar. Note that the peaks in the density profile correspond to the troughs in the magnetization profile. This agrees with the linear stability analysis, wherein disturbances in the density give rise to disturbances in the magnetization.

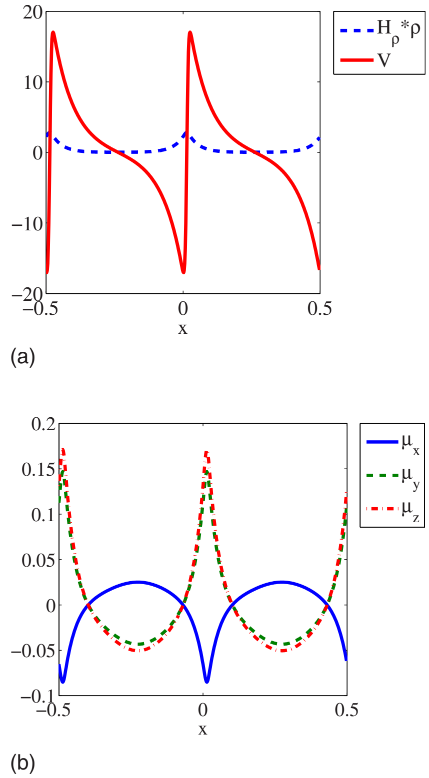

FIG. 10. (Color online) Evolution of sinusoidally varying initial conditions for the density and magnetization, as in Eq. (22). (a) shows the system velocity V given in Eq. (12), just before the singularity time; (b) shows the magnetization $\boldsymbol{\mu}$ at the same time. The density maxima emerge at the locations where the convergence of $-V$ (flow into $x=0$ and $x=\pm L/2$) occurs, and the magnetization develops extrema there.

$$\frac{\partial \theta}{\partial t} = \lambda_0 x \frac{\partial \theta}{\partial x}, \quad \lambda_0 > 0.$$

Given initial data $\theta(x,0)=\theta_0 e^{-x^2/\ell_0^2}$, the solution evolves in time as

$$\theta(x,t) = \theta_0 e^{-x^2/(\ell_0^2 e^{-2\lambda_0 t})},$$

so that gradients are amplified exponentially in time,

$$\frac{\partial \theta}{\partial x} = -\frac{2\theta_0}{\ell_0^2} x e^{\lambda_0 t} e^{-x^2/(\ell_0^2 e^{-2\lambda_0 t})},$$

in a similar manner to the problem studied.

The evolution of the set of initial conditions (22) has therefore demonstrated the following: the local velocity V is such that before the onset of the singularity, matter is compressed into regions where $\rho(x,0)$ is large, to such an extent that the matter eventually accumulates at isolated points, and the singular solution emerges. Moreover, the density maxima, rather than the magnetization extrema, drive the formation of singularities. This is not surprising, given that the attractive part of the system's energy comes from density variations.

To highlight the interaction between clumpons, we examine the following set of initial conditions:

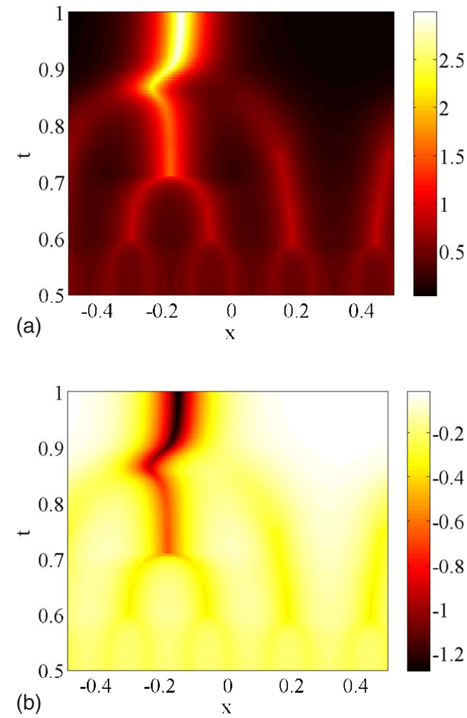

FIG. 11. (Color online) Evolution of a flat magnetization field and a sinusoidally varying density, as in Eq. (23). (a) shows the evolution of $H_\rho * \rho$ for $t \in [0.5,1]$; (b) shows the evolution of μ_x. The profiles of μ_y and μ_z are similar. At $t=0.5$, the initial data have formed eight equally spaced, identical clumpons, corresponding to the eight density maxima in the initial configuration. By impulsively shifting the clumpon at $x=0$ by a small amount, the equilibrium is disrupted and the clumpons merge repeatedly until only one clumpon remains.

$$\boldsymbol{m}(x,0) = \boldsymbol{m}_0 = \text{const}, \quad \rho(x,0) = 0.5 + 0.35\cos(8k_0 x), \tag{23}$$

where $k_0 = 2\pi/L$ is the fundamental wave number. Since this set of initial conditions contains a large number of density maxima, we expect a large number of closely spaced clumpons to emerge, and this will illuminate the clumpon interactions. The time evolution of equations (10) for this set of initial conditions is shown in Fig. 11. As before, the solution becomes singular after a short time, and is subsequently represented by a sum of clumpons,

$$\rho(x,t) = \sum_{i=1}^{M} a_i \delta(x - x_i(t)), \quad \boldsymbol{m}(x,t) = \sum_{i=1}^{M} \boldsymbol{b}_i(t)\delta(x - x_i(t)),$$

$$M = 8.$$

Here $M=8$ is the number of clumpons at the singularity time. This number corresponds to the number of maxima in the initial density profile. As before, this configuration of equally spaced, identical clumpons is an equilibrium state, due to periodic boundary conditions. Therefore, once the particle-like state has formed, we impulsively shift the clumpon at $x=0$ by a small amount, and precipitate the merging of clumpons. (See Fig. 12). The eight clumpons then merge

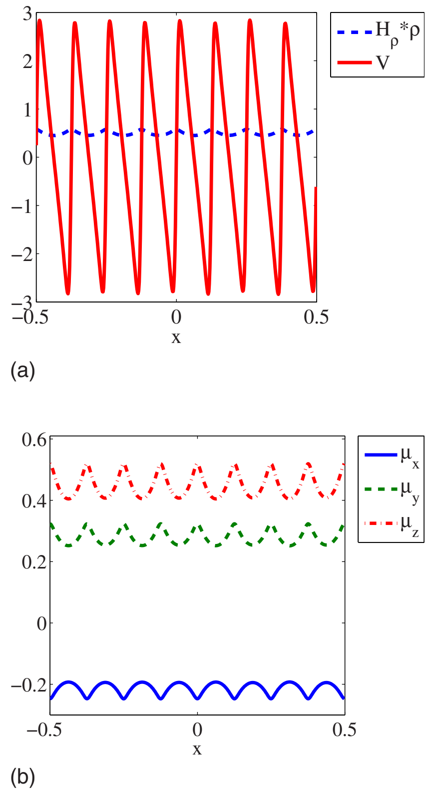

FIG. 12. (Color online) Evolution of a flat magnetization field and a sinusoidally varying density, as in Eq. (23). (a) shows the system velocity V given in Eq. (12) just before the singularity time; (b) gives the magnetization $\boldsymbol{\mu}$ at the same time. The density maxima emerge at the locations where the convergence of $-V$ occurs, and the magnetization develops extrema there.

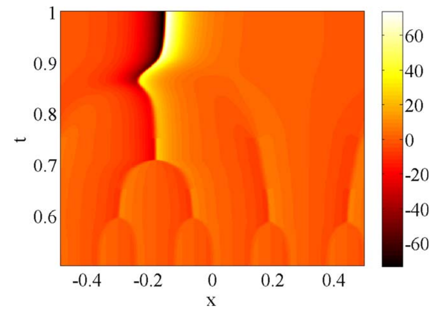

FIG. 13. (Color online) Evolution of a flat magnetization field and a sinusoidally varying density, as in Eq. (23). Shown is the velocity profile for $t\in[0.5,1]$; the system velocity is given by Eq. (12). The velocity $-V$ flows into each density maximum, concentrating matter at isolated points and precipitating the formation of eight equally spaced identical clumpons. On a periodic domain, such an arrangement is an equilibrium state, although it is unstable. Thus, by impulsively shifting the clumpon at $x=0$ by a small amount, we force the clumpons to collapse into larger clumpons, until only a single clumpon remains.

repeatedly until only a single clumpon remains. The tendency for the clumpons to merge is explained by the velocity V, which changes sign across a clumpon. Thus, if a clumpon is within the range of the force exerted by its neighbors, the local velocity, if unbalanced, will advect a given clumpon in the direction of one of its neighbors, and the clumpons merge. This process is shown in Fig. 13.

It is important to emphasize that the role of periodic boundary conditions here should not be overestimated. Once the unstable multiclumpon equilibrium state has been accounted for, the effect of the periodic boundary conditions is unimportant, and our choice of boundary conditions is representative of the infinite medium. This agrees with the purpose of this paper, which presents the clumpon-clumpon interaction, without the involvement of other external forces. Indeed, the results presented here are always valid as long as the clumpons are far enough from the boundary so that there is no interaction between clumpons and the boundary.

IV. CONCLUSIONS

We have investigated the nonlocal Gilbert (NG) equation introduced by Holm, Putkaradze, and Tronci in [6] using a combination of numerical simulations and simple analytical arguments. The NG equation contains two competing length scales of nonlocality: there is a length scale α associated with the range of the interaction potential, and a length scale β that governs the smoothened magnetization vector that appears in the equation. When $\alpha<\beta$ all initial configurations of the magnetization tend to a constant value, while for $\beta<\alpha$ the initial configuration of the magnetization field develops finer and finer scales. These two effects are in balance when $\alpha=\beta$, and the system does not evolve away from its initial state. Furthermore, the NG equation conserves the norm of the magnetization vector $\boldsymbol{m}$, thus providing a pointwise bound on the solution and preventing the formation of singular solutions.

To study the formation of singular solutions, we couple the NG equation to a scalar density equation. Associated with the scalar density is a negative energy of attraction that drives the formation of singular solutions and breaks the pointwise bound on the $\boldsymbol{m}$. Three length scales of nonlocality now enter into the problem: the range of the force associated with the scalar density, the range of the force due to the magnetization, and the smoothening length. As before, the competition of length scales is crucial to the evolution of the system; this is seen in the linear stability analysis of the coupled equations, in which the relative magnitude of the length scales determines the stability or otherwise of a constant state.

Using numerical simulations, we have demonstrated the emergence of singular solutions from smooth initial data, and have explained this behavior by the negative energy of attraction produced by the scalar density. The singular solution consists of a weighted sum of delta functions, given in Eq. (17), which we interpret as interacting particles or clumpons. The clumpons evolve under simple finite-dimensional dynamics. We have shown that a system of two clumpons is governed by a two-dimensional dynamical system that has a multiplicity of steady states. Depending on the length scales of nonlocality and the clumpon weights, the two clumpons can merge, diverge, or align and remain separated by a fixed distance. Similarly, one can consider three-particle collisions, which are not presented in this paper. The treatment for the simultaneous collision of three clumpons or more requires no change with respect to the approach presented here. Also, when the number of clumpons is sufficiently large, the system might be related with coarsening dynamics. However, our results are restricted to a small number of clumpons and thus shed no light on coarsening laws. In particular, the results in this paper depend on the initial positions of the clumpons and show no self-similarity or scaling law behavior.

Our paper thus gives a qualitative description of the dynamics. Future work will focus on the regularity of solutions of the NG equation, and the existence and regularity of solutions for the coupled density-magnetization equations. Bertozzi and Laurent [29] have studied the simpler (uncoupled) nonlocal scalar density equation, proving existence, uniqueness, and blowup results using techniques from functional analysis, and a similar analysis will illuminate the equations we have studied. Interestingly, localized particle type solutions have recently shown to appear also in nonlocal population dynamics [30]. Another issue is the insertion of a stochastic source in the equations: this modifies the emergence of singular solutions and is a topic of future research.

ACKNOWLEDGMENTS

D.D.H. was partially supported by the US Department of Energy, Office of Science, Applied Mathematical Research, and the Royal Society. C.T. was also partially supported by the Royal Society. Support by the European network MISGAM is also acknowledged. L.Ó.N. was supported by the Irish government and the UK Engineering and Physical Sciences Research Council.

[1] F. A. Denis, P. Hanarp, D. S. Sutherland, and Y. F. Dufrêne, Nano Lett. **2**, 1419 (2002).
[2] J. G. Veinot, H. Yan, S. M. Smith., J. Cui, Q. Huang, and T. J. Marks, Nano Lett., **2**, 333 (2002).
[3] R. Möller, A. Csáki, J. M. Köhler, and W. Fritzsche, Langmuir **17**, 5426 (2001).
[4] J. E. G. J. Wijnhoven and W. L. Vos, Science **281**, 802 (1998).
[5] E. Wolf, *Nanophysics and Nanotechnology* (Wiley-VCH, Weinheim, 2004).
[6] D. D. Holm, V. Putkaradze, and C. Tronci, e-print arXiv:0707.4204.
[7] D. D. Holm, V. Putkaradze, and C. Tronci, C. R. Math. **345**, 297 (2007).
[8] D. D. Holm, V. Putkaradze, and C. Tronci, e-print arXiv:0704.2369, Physica D (to be published).
[9] D. D. Holm and V. Putkaradze, Physica D **235**, 33 (2007).
[10] D. D. Holm and V. Putkaradze, Physica D **220**, 183 (2006).
[11] D. D. Holm and V. Putkaradze, Phys. Rev. Lett. **95**, 226106 (2005).
[12] S. Chandrasekhar, *An Introduction to the Theory of Stellar Structure* (Dover, New York, 1939).
[13] E. F. Keller and L. A. Segel, J. Theor. Biol. **26**, 399 (1970).
[14] S. A. Levin and L. A. Segel, SIAM Rev. **27**, 45 (1985).
[15] C. M. Topaz, A. L. Bertozzi, and M. A. Lewis, Bull. Math. Biol. **68**, 1601 (2006).
[16] K. Mertens, V. Putkaradze, D. Xia, and S. R. Brueck, J. Appl. Phys. **98**, 034309 (2005).
[17] D. Xia and S. Brueck, Nano Lett. **4**, 1295 (2004).
[18] D. D. Holm, V. Putkaradze, and C. Tronci, e-print arXiv:0712.0397, J. Phys. A (to be published).
[19] M. G. Forest, R. Zhou, and Q. Wang, IJNAM **4**, 478 (2007).
[20] T. L. Gilbert, IEEE Trans. Magn. **40**, 3443 (2004).
[21] E. Weinan and W. Xiao-Ping, SIAM (Soc. Ind. Appl. Math.) J. Numer. Anal. **38**, 1647 (2000).
[22] J. D. Murray, *Mathematical Biology* (Springer-Verlag, Berlin, 1989).
[23] J. Zhu, L. Q. Chen, J. Shen, and V. Tikare, and Phys. Rev. E **60**, 3564 (1999).
[24] S. Chandrasekhar, *Hydrodynamic and Hydromagnetic Stability* (Dover, New York, 1961).
[25] M. Argentina, M. G. Clerc, R. Rojas, and E. Tirapegui, Phys. Rev. E **71**, 046210 (2005).
[26] J. Garcia-Ojalvo and J. Sancho, *Noise in Spatially Extended Systems* (Springer, New York, 1999).
[27] S. H. Strogatz, *Nonlinear Dynamics and Chaos* (Perseus Books Group, New York, 2001).
[28] G. K. Batchelor, J. Fluid Mech. **5**, 113 (1959).
[29] A. L. Bertozzi and T. Laurent, Commun. Math. Phys. **274**, 717 (2007).
[30] M. G. Clerc, D. Escaff, and V. M. Kenkre, Phys. Rev. E **72**, 056217 (2005).